Time Reversal Focusing and Imaging of Point-Like Defects in Specimens with Nonplanar Surface Geometry

Hyunjo Jeong*†, Hyun-Kee Lee*, Sung-Min Bae* and Jung-Sik Lee*

Abstract Nonplanar surface geometries of components are frequently encountered in real ultrasonic inspection situations. Use of rigid array transducers can lead to beam defocusing and reduction of defect image quality due to the mismatch between the planar array and the changing surface. When a flexible array is used to fit the complex surface profile, the locations of array elements should be known to compute the delay time necessary for adaptive beam focusing. An alternative method is to employ the time reversal focusing technique that does not require a prior knowledge about the properties and structures of the specimen and the transducer. In this paper, a time reversal method is applied to simulate beam focusing of flexible arrays and imaging of point-like defects contained in specimens with nonplanar surface geometry. Quantitative comparisons are made for the performance of a number of array techniques in terms of the ability to focus and image three point-like reflectors positioned at regular intervals. The sinusoidal profile array studied here exhibits almost the same image quality as the flat, reference case.

Keywords: Nonplanar Surface, Flexible Array, Beam Focusing, Time Reversal, Image Quality

1. Introduction

Ultrasonic phased array transducers are widely used for nondestructive evaluation(NDE) and for many medical applications(Azar et al., 2000; Poguet et al., 2002; Holmes et al., 2002). Some of the attractive features of phased arrays include electronic focusing and steering capabilities. Beam steering to test objects with multiple angles from a single probe can greatly simplify the inspection of components with complex geometries, thus can greatly increase the probability of detection of anomalies. The ability to narrowly focus the beam provides enhanced spatial resolution for flaw detection and sizing. Focusing can also significantly improve signal-to-noise ratio in challenging applications.

To generate a focused beam at any specified angle and distance, time delays are calculated and applied electronically to each element. However, these techniques suffer important limitations. They are all based on a priori knowledge of geometry and acoustic properties of the sample and assume that the sound velocity is known and constant in each medium.

Nonplanar surface geometries of components are frequently encountered in real inspection situations (e.g., butt weld, nozzle, elbow). Coupling a conventional rigid array with a specimen can be difficult when its surface is changing. The mismatch creates an irregular coupling layer between the planar array and the local surface, and can lead to beam defocusing and a reduction of image quality. Some imaging

parameters, such as the array geometry, propagation speeds, etc., can be measured physically. Flexible phased arrays have been developed to fit the complex profile and improve the defect imaging(Casula et al., 2006a; Casula et al., 2006b; Toullelan et al., 2008). The radiating surface is composed of piezoelectric elements mechanically assembled and a profilometer measures the local profile of components. The computed locations are used to compute the delay time necessary for each element for adaptive beam focusing. However, the additional hardware may increase the size and cost of the device and might not provide the required positional accuracy. An alternative method is to employ the time reversal focusing technique that does not require a prior knowledge about the properties and structures of the media and the transducer.

One of the fundamental features of time reversal(TR) techniques is the ability to focus interrogating beams on the source location within the test material. Narrowly focusing the beam can provide enhanced spatial resolution for flaw detection and sizing. Focusing can also significantly improve signal-to-noise ratio in challenging applications. Recent application areas include underwater acoustics, biomedical ultrasound imaging and therapy, nondestructive evaluation, and seismology(Chakroun et al., 1995; Ing and Fink, 1996; Ing et al., 1996; Ing and Fink, 1998; Tournat et al., 2006). Recently, Jeong (Jeong et al., 2008; Jeong, 2009 Jeong et al., 2009a; Jeong et al., 2009b) investigated the TR beam focusing and steering behavior of array transducers composed of multiple rectangular elements using a multi-Gaussian beam(MGB) model. A typical TR focusing and imaging procedure can be realized in the following way (Fig. 1): (a) One of the array elements is (or all array elements are) first excited as an unfocused array. (b) Backscattered signals are recorded by the elements of the array, time-reversed, and then re-emitted at the same time, (c) The wave back-propagates through the medium and focuses on the initial source location. (d) Finally defect localization imaging is obtained through the post processing of received element data.
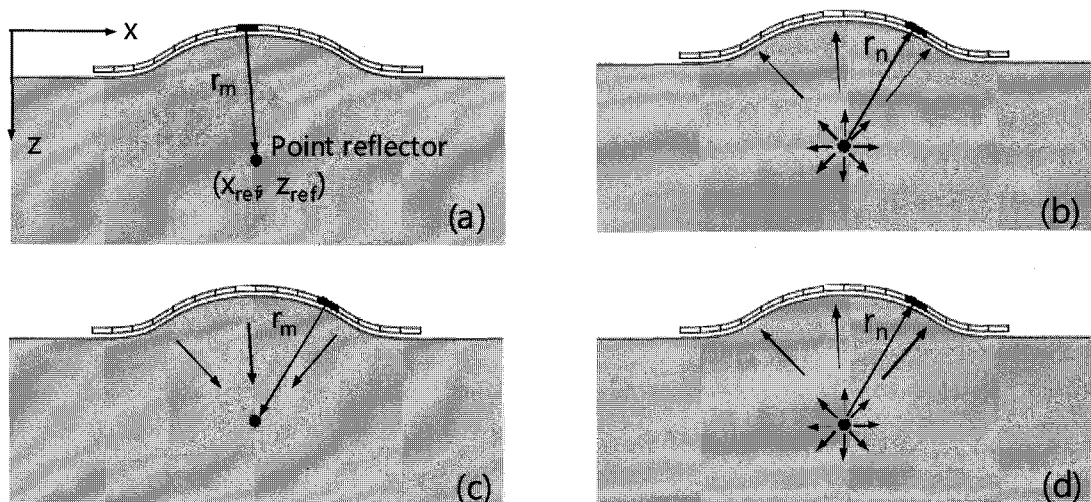

Fig. 1   Principle of time reversal focusing and imaging of a point reflector: (a) One of the array elements is (or all array elements are) fired first, (b) Backscattered signals from the reflector are recorded by each element of the array, (c) Received signals are time-reversed and re-emitted simultaneously. The wave back-propagates through the medium and focuses on the initial reflector position, (d) Backscattered signals from the reflector are recorded by each element and further processed for defect localization imaging

In this paper, we consider the TR focusing and imaging through a nonplanar surface geometry with a flexible ultrasonic array. A two-dimensional simulation program was written to describe the beam field of the individual time domain traces for all combinations of transmitter and receiver elements. A beamforming method was then used to construct a defect localization image (location and imaging) by relating the contrast at a particular pixel to the amplitude of the scattered signal received by all the elements in the array. Quantitative comparisons are made for the performance of array techniques in terms of the ability to detect and image point-like reflectors through a sinusoidal interface.

2. Description of Array Transducer Wave Fields

This section describes the model which will be used to simulate the ultrasonic array system. We assess the performance of time reversal array techniques and their ability to detect and image point-like reflectors through a non-planar interface. More specifically, the TR focusing and imaging through a nonplanar surface geometry will be considered with application to a flexible ultrasonic array.

In the first step of time reversal focusing and imaging, one of the array elements is (or all the elements are) fired and the scattered signal from the point reflector is received by all elements of the array. The transducer wave field radiated from a rectangular element of lengths $2a_1$ and $2a_2$ at the point reflector position r_m (Fig. 2(a)) can be written in the form of a quasi-plane wave velocity as

$$V(r_m, \omega) = B(\omega) C(r_m, a_1, a_2, \omega) e^{ikr_m} \quad (1)$$

where $k = \omega/c$ is the wave number of P-wave of velocity c, ω is the circular frequency, $B(\omega)$ is the transducer output, and $C(r, a_1, a_2, \omega)$ is a diffraction coefficient. The diffraction coefficient accounts for all the deviations in amplitude and phase of the actual transducer beam from that of plane wave. Here, the diffraction coefficient is obtained from the multi-Gaussian beam model for a rectangular transducer(Jeong et al., 2008). This diffraction coefficient takes into account the directivity of a contact transducer and provides the entire wave fields of a planar rectangular piston transducer. The scattered wave field received at the nth element of the array due to the point reflector (Fig. 2(b)) is similarly given by

$$V_n(r_n, \omega) = V(r_m, \omega) C_n(r_n, a_1, a_2, \omega) e^{ikr_n} \quad (2)$$

The position of a point reflector within the sample is defined by the coordinates $(x, z) = (x_{ref}, z_{ref})$. The propagation distance, r_m, from one of the array elements to the reflector is then calculated as follows:

$$r_m = \sqrt{(x_m - x_{ref})^2 + (z_m - z_{ref})^2} \quad (3)$$

The propagation distance, r_n, from the point reflector to the nth receiver is given by

$$r_n = \sqrt{(x_n - x_{ref})^2 + (z_n - z_{ref})^2} \quad (4)$$

In the second step of TR, the recorded signals are time reversed and reemitted simultaneously by each element. After TR, the signals radiated by different elements arrive synchronously in phase. Thus, they are enhanced by each other and refocused. The velocity field for each element will be calculated in the frequency domain, therefore it will be given by a complex value. Time reversal operation is the same as phase conjugation. The time reversal operation at the focal point is then performed by taking the complex conjugate of the received velocity. This quantity of complex conjugate will be referred to as "TR coefficient" here. The TR coefficient is then multiplied as an input parameter when the beam is reradiated all together from the N elements at the initial transducer position. The

total beam fields after the TR process can be obtained by simply superposing the individual field (Fig. 2(c)). For a linear phased array transducer with N elements, the P-wave velocity field is then calculated by

$$V_{total}(\omega) = \tag{5}$$

$$\sum_{m=1}^{N} \sum_{n=1}^{N} V_n^*(r_n,\omega) C_m(r_m,a_1,a_2,\omega) e^{ikr_m}$$

where $V_n^*(r_n,\omega)$ is the TR coefficient, and ( )* denotes the complex conjugate.

Finally the received signal of each element due to the focused beam scattering from the reflector (Fig. 2(d)) is given by

$$H_n(r_n,\omega) = V_{total}(\omega) C(r_n,a_1,a_2,\omega) e^{ikr_n} \tag{6}$$

An inverse Fourier transform can then be applied to transform the signal back to the time domain, $h_n(r_n,t)$, but in practice it is more convenient for subsequent defect localization image to obtain the envelope of the received signal using Hilbert transform(Jang et al., 1999):

$$h_n(r_n,t) = \frac{1}{\pi} \int_0^\infty H_n(r_n,\omega) e^{-iwt} dw \tag{7}$$

3. Beamforming for Defect Imaging

A beamforming method can be used to construct a defect localization image (location and imaging) by relating the contrast at a particular pixel to the amplitude of the scattered signal received by all the sensors in the array. Consider a linear array consisting of N active elements, their positions being denoted by (x_n,z_n), n=1, 2, . . . N. The contrast S at a particular location or imaging pixel (x, z) can be expressed as

$$S(x,z) = \sum_{n=1}^{N} h_n(t_n(x,z)) \tag{8}$$

where $h_n(t_n)$ denotes the received signal amplitude of element n. Referring to Fig. 1, the

arrival time t_n of the received wave at the nth element corresponds to the wave travel time from the transmitting element to the reflector and then from the reflector to the same receiving element, and is given by

$$t_n(x,z) = \frac{2\sqrt{(x_n-x)^2+(z_n-z)^2}}{c} \tag{9}$$

For isotropic materials, imaging pixels with identical relative amplitude form ellipses for each array element. The defect localization image is created by superimposing the received signals after TR reradiation and backscattering from point reflectors. In the present study, an array transducer with 64 elements is employed, so that a total of 64 pulse-echo type received signals will be obtained and used for defect imaging.

4. Simulation Results and Discussion

Two test specimens are considered to study three point reflectors and shown in Fig. 2. The specimens are steel blocks with the longitudinal wave speed of 5900 m/s, the shear wave speed of 3200 m/s and the density of 7.9 kg/m^3. The first specimen has a planar surface to simulate a flat, reference array, as shown in Fig. 2(a). The second specimen has a surface with a sinusoidal profile of amplitude ±2.5 mm and period 40 mm, as shown in Fig. 2(b). The second specimen is to simulate a flexible array. The position of three point reflectors within the specimen is defined in terms of the x, y and z coordinates, located at (-20, 0, 60), (-10, 0, 50), (0, 0, 40), (10, 0, 30), and (20, 0, 20) mm relative to the center of the array transducer. In the present study, multiple scattering from point reflectors, and reflections from specimen boundaries are ignored.

The array geometry used for the modeling is that of a linear array transducer with equi-spaced elements. As an example the operation of a typical commercial 5 MHz array with 64 elements was modeled. The array has an element pitch of 0.625 mm and a total length of 40 mm.

The size of rectangular element is (2a_1, 2a_2)=(1.25, 10) mm in the x- and y-directions. The output signal of each element has a center frequency of 5 MHz and a -6 dB bandwidth of 50%.
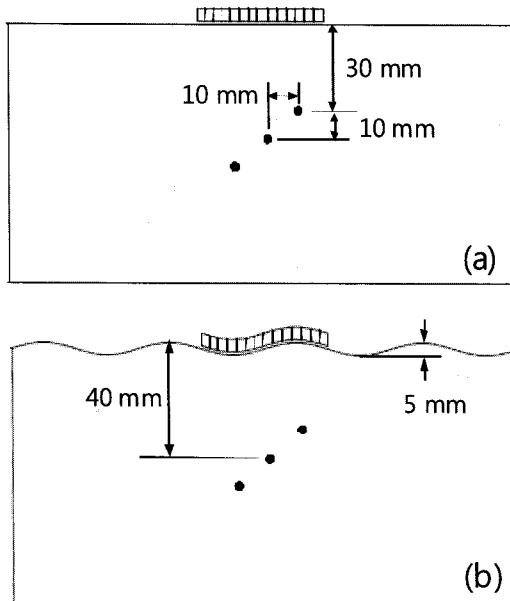

Fig. 2 Specimen geometry for simulation: (a) Planar surface for a flat array simulation, and (b) Sinusoidal surface for a flexible array simulation

When all the 64 elements are radiated simultaneously without time reversal focusing, the resulting beam fields in the x-z plane are shown in Fig. 3(a)-(b). In the flat array case, the transition range of an array transducer is defined, in a similar manner to a single transducer, as (Jeong et al., 2008; Jeong, 2009)

$$Z_{TR} = \frac{D^2}{4\lambda} \tag{10}$$

where D is the overall dimension of the array transducer, and λ is the wavelength. This transition range separates the near field from the far field of the array. It is known that focusing of array transducers may increase the system resolution for imaging targets that are located within the near field of the array aperture, that is, at distances less than Z_{TR}. For the current

setup of the array transducer, Z_{TR} is calculated as 339 mm, and the simulation, Fig. 3(a2), accurately predicts this value. Fig. 3(b) shows the beam field of the flexible array case when all the 64 elements are fired at the same time without TR focusing. It can be seen that, as expected, the geometric focusing occurs in front of the concave surface profile.

Using the array described above, the time reversal focusing algorithm described in eqn. (5) was applied and the reconstructed reflector images were assessed for a number of surface geometry. Two different surface geometries (or arrays) were considered - flat and sinusoidal profiles. Actually, a total of three different cases are studied by combining the surface geometry and the TR focusing, i.e. flat array for both TR focusing and reflector imaging, flat array for TR focusing and sinusoidal array for reflector imaging, and the sinusoidal array for both TR focusing and reflector imaging. For each of these cases, 2-D cross-sections of the TR focused wave field and the reflector image were produced for point reflectors positioned at regular intervals in the x-z plane.

Fig. 4 shows 2-D cross-sections of the TR focused wave field and the reflector image obtained for the first case considered (flat array for both TR focusing and reflector imaging). The TR focused wave field shows three focused regions at the initial reflector positions. It is noticed that the focal strength increases and the focal spot size decreases as the position of a reflector moves toward the center line of the array, as previously observed(Jeong et al., 2008; Jeong, 2009). Because of this focusing behavior, the three reflectors are well separated and clearly visible. The central reflector has the maximum response of image magnitude, so that this peak magnitude will be used as a reference value for assessing the image quality of point reflectors in other cases.

The second case deals with the specimen with the sinusoidal surface. A flat array profile of the first case was assumed for calculation of

the time reversal coefficient. The actual sinusoidal geometry was then used for simultaneous reradiation of time reversed wave fields and reception of scattered waves. The simulated results are shown in Fig. 5 for TR focused field and reconstructed reflector image. Since the flat array was assumed for TR focusing, the focused wave field does not produce any focal spots at the reflector positions. Because of this poor focusing behavior, the peak magnitudes of reflector images are reduced by more than 14 dB, as assessed below. Moreover, some of the reflectors are not easily distinguished. Extra images are also generated near the original reflector positions. These images may be artifacts due to the geometrical focusing.

The third case simulated the sinusoidal specimen when the actual surface geometry was used for TR focusing as well as reflector image

reconstruction. TR focused wave field and reconstructed reflector images are shown in Fig. 6. The TR focusing behavior is similar to the flat array case. It is found that using the actual surface profile provides a significant improvement in the image quality. The three reflectors are now clearly defined due to the correct focusing.

A summary of the reflector magnitudes in the reconstructed images of three different cases is given in Table1. The first column in the maximum magnitude of image in Table 1 represents the reference specimen with flat surface. The image magnitude (in dB) is relative to the maximum response of the central reflector. The image magnitudes of reflectors in the other two cases are also calculated with respect to the maximum response of this central reflector.

The second column of the maximum image magnitude represents the specimen with the
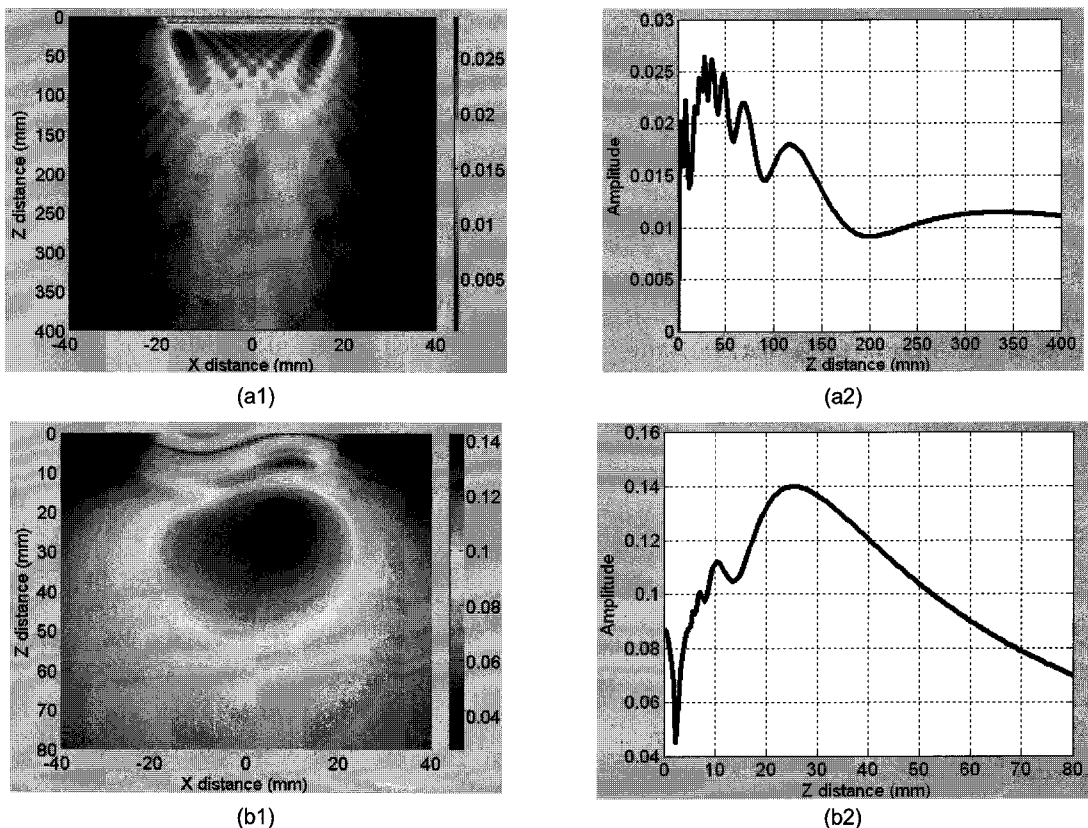

(a1)

(a2)

(b1)

(b2)

Fig. 3 2-D beam profile and the on-axis wave field when all the 64 elements are radiated at the same time without focusing: (a) The flat array, and (b) The flexible array
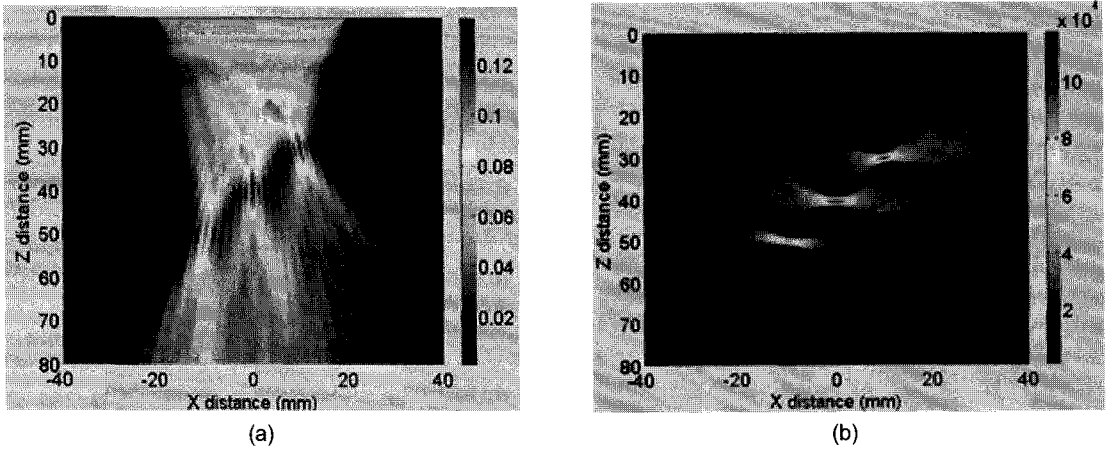
(a)

(b)

Fig. 4   Simulation results for the specimen with the flat surface profile: (a) TR focused wave field, and (b) The image of three point reflectors
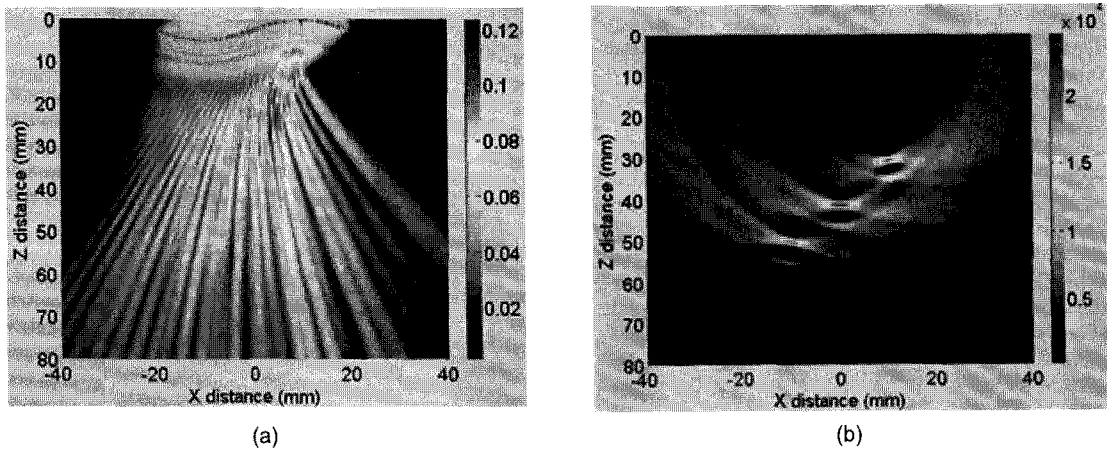

(a)

(b)

Fig. 5   Simulation results for the specimen with the sinusoidal surface profile: (a) TR focused wave field with the flat geometry assumed, and (b) The image of three point reflectors
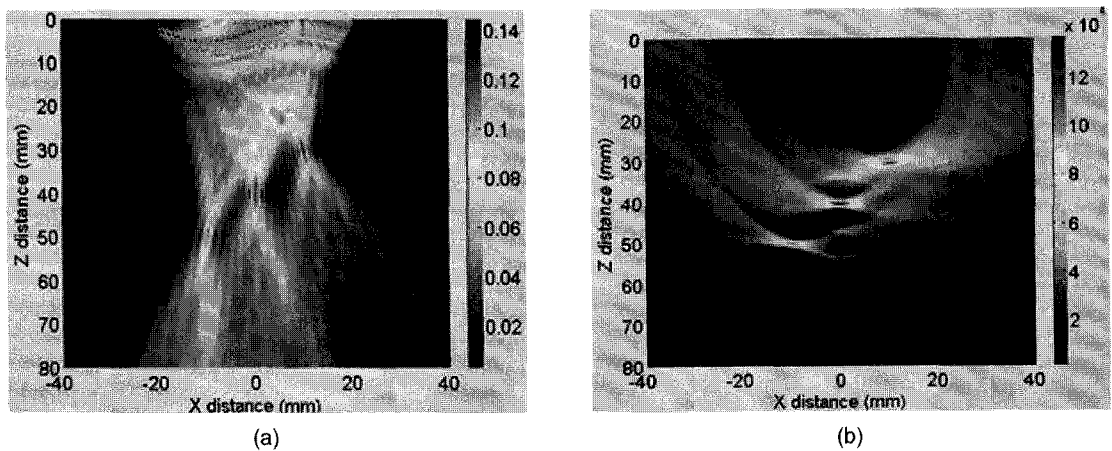

(a)

(b)

Fig. 6   Simulation results for the specimen with the sinusoidal surface profile: (a) TR focused wave field with the actual geometry used, and (b) The image of three point reflectors

Table 1 A summary of the reflector image magnitudes obtained from the simulated data for three point reflectors

Reflector location (mm)	Maximum magnitude of reflector image (dB)		
	Flat surface profile Flat surface	Sinusoidal surface profile	
		Flat surface assumption (Fig. 5b)	Actual surface geometry (Fig. 5c)
(-10, 0, 50)	-2.4	-15.7	-1.4
(0, 0, 40)	0	-13.8	0.7
(10, 0, 30)	-0.9	-15.3	-0.5

sinusoidal surface. However, a flat array profile was assumed for calculation of the time reversal coefficient, as described earlier. The actual sinusoidal geometry was then used for reception of scattered signal after TR focusing and reconstruction of the reflector image. Again, the image magnitude is relative to the central reflector in the reference image. Since the flat array was assumed for TR focusing and it does not conform to the actual surface geometry, the peak image magnitude is found to be reduced by more than 14 dB.

The third column represents the maximum image magnitude of three reflectors of the sinusoidal specimen when the actual surface geometry was used for TR focusing as well as reflector image reconstruction. Again, the image magnitude is relative to the central reflector in the reference image. Use of the actual surface profile demonstrates a significant improvement in the image quality. The maximum magnitude of image for the sinusoidal surface case (third column) exhibits a slightly better overall image quality than the reference image (first column). The main reason for this improvement might be due to the geometrical focusing effect of the current sinusoidal surface in addition to the actual TR focusing.

5. Conclusion

A time reversal (TR) technique was applied to investigate the ultrasonic beam focusing and imaging of defects contained in a specimen with

nonplanar surface geometry. The flexible array beam focusing and imaging of equally spaced point reflectors in a specimen with sinusoidal interface was simulated using the multi-Gaussian beam model. The simulation results demonstrated that almost the same quality of reflector images could be obtained for the sinusoidal specimen when compared to the reflector images of the same specimen with planar surface. The present study used the known surface profile for TR focusing and imaging. However, the TR focusing technique, in principle, does not require knowledge about the array geometry or acoustic properties of specimen. Therefore, the proposed technique, in principle, can be applied to any unknown array geometry with application to a flexible array. The technique can also be extended to the estimation of unknown imaging parameters, e.g., the propagation speeds in inhomogeneous or anisotropic materials.

References

Azar, L., Shi, Y. and Wooh, S. C. (2000) Beam Focusing Behavior of Linear Phased Arrays, *NDT&E International*, Vol. 33, pp. 189-198

Casula, O., Poidevin, C., Cattiaux, G. and Dumas, Ph. (2006a) Control of Complex

Components with Smart Flexible Phased Arrays, *Review of Progress in QNDE*, vol. 25, pp. 829-836

Casula, O., Poidevin, C., Cattiaux, G. and Dumas, Ph. (2006b) Control of Complex Components with Smart Flexible Phased Arrays, *Ultrasonics*, Vol. 44, pp. 647-651

Chakroun, N., Fink, M. and Wu, F. (1995) Time Reversal Processing in Ultrasonic Nondestructive Testing, *IEEE Trans. Ultrason. Ferroelectr. Freq. Control*, Vol. 42, pp. 1087-1098

Holmes, C., Drinkwater, B. W. and Wilcox, P. (2005) Post-Processing of the Full Matrix of Ultrasonic Transmit-Receive Array Data for Non-Destructive Evaluation, *NDT&E International*, Vol. 38, pp. 701-711

Ing, R. K. and Fink, M. (1996) Time Recompression of Dispersive Lamb Waves Using a Time Reversal Mirror–Application to Flaw Detection in Thin Plates, *IEEE Ultrason. Symp.*, Vol. 1, pp. 659-663

Ing, R. K. and Fink, M. (1998), Time-Reversed Lamb Waves, *IEEE Trans. Ultrason. Ferroelectr. Freq. Control*, Vol. 45, pp. 1032-1043

Ing, R. K., Fink, M. and Casula, O. (1996) Self-Focusing Rayleigh Wave Using a Time Reversal Mirror, *Appl. Phys. Lett.* 68, pp. 161-163

Jeong, H., Lee, J.-S., Jeong Y.-H. and Bae, S.-M. (2008) On the Beam Focusing Behavior of Time Reversed Ultrasonic Arrays Using a Multi-Gaussian Beam Model, *Journal of the Korean Society for Nondestructive Testing*, Vol. 28, No. 6, pp. 521-537

Jeong, H. (2009) Ultrasonic Beam Focusing and Steering of Array Tansducers Based on a

Time-Reversal Process, *Materials Evaluation*, Vol. 67, pp. 721-729

Jeong, H., Lee, J.-S. and Bae, S.-M. (2009a) Time Reversal Beam Focusing of Ultrasonic Array Transducer on a Defect in a Two Layer Medium, *Journal of the Korean Society for Nondestructive Testing*, Vol. 29, No. 3, pp. 242-247

Jeong, H., Lee, J.-S., Lee, C.-H. and Jun, G.-C. (2009b) Time Delay Focusing of Ultrasonic Array Transducers on a Defect Using the Concept of a Time Reversal Process, *Journal of the Korean Society for Nondestructive Testing*, Vol. 29, No. 6, pp. 550-556

Jang, Y.-S., Kim, J.-H., Jeong, H. and Nam, Y.-H. (1999) Measurement of Ultrasonic Velocity and Attenuation by Signal Processing Techniques in Time and Frequency Domains, *Journal of the Korean Society for Nondestructive Testing*, Vol. 19, No. 2, pp. 118-128

Poguet, J., Marguet, J., Pichonnat, F. and Chupin, L. (2002) Phased Array Technology: Concepts, Probes and Applications, NDT.net, Vol. 7, No. 5

Tournat, V., Profunser, D. M., Muramoto, E., Matsuda, O., Takezaki, T., Sueoka, S. and Wright, O. B. (2006) Microscale Multiple Scattering of Coherent Surface Acoustic Wave Packets Probed with GHz Time-Reversal Acoustics, *Phys. Rev. E 74*, 026604/1-5

Toullelan, G., Casula, O., Abittan, E. and Dumas, Ph. (2008) Application of a 3D Smart Flexible Phased-Array to Piping Inspection, *Review in Progress in QNDE*, Vol. 27, pp. 794-795